INVITED PAPER

Multiscale Modeling for Graphene-Based Nanoscale Transistors

In this paper, the authors review multiscale modeling of graphene transistors. The importance of quantum effects is discussed, as well as ab initio methods for modeling of graphene and graphene nanoribbon-based transistors.

By Gianluca Fiori and Giuseppe Iannaccone, *Senior Member IEEE*

ABSTRACT | The quest for developing graphene-based nanoelectronics puts new requirements on the science and technology of device modeling. It also heightens the role of device modeling in the exploration and in the early assessment of technology options. Graphene-based nanoelectronics is the first form of molecular electronics to reach real prominence, and therefore the role of single atoms and of chemical properties acquires more relevance than in the case of bulk semiconductors. In addition, the promising perspectives offered by band engineering of graphene through chemical modifications increase the role of quantum chemistry methods in the assessment of material properties. In this paper, we review the multiphysics multiscale (MS) approaches required to model graphene-based materials and devices, presenting a comprehensive overview of the main physical models providing a quantitative understanding of the operation of nanoscale transistors. We especially focus on the ongoing efforts to consistently connect simulations at different levels of physical abstraction in order to evaluate materials, device, and circuit properties. We discuss various attempts to induce a gap in graphene-based materials and their impact on the operation of different transistor structures. Finally, we compare candidate devices in terms of integrated circuit performance and robustness to process variability.

KEYWORDS | Computational electronics; electron devices; graphene; multiscale (MS) modeling; nanoelectronics; nanoscale transistors

I. INTRODUCTION

Carbon-based electronics is a remarkable scientific domain, amenable to different and partially overlapping descriptions of the physical world. On the one hand, graphene monolayers and carbon nanotubes are very large molecules, apt to be investigated with the conceptual and experimental tools of chemistry. On the other hand, they are large enough to be treated as low-dimensional solid-state structures, using familiar concepts as energy dispersion relations and semiclassical particle-based transport equations.

In addition, the chemical and physical properties of carbon-based materials can be engineered—through the use of new materials or, for example, with chemical functionalization—to optimize device performance and technology potential. This requires control of single atoms and complete understanding of their role, which in turn must be based on full mastery of chemical synthesis and solid-state fabrication technology.

The main challenge is that experimental techniques are not sufficiently mature and reproducible to allow the realization of high performing and reliable devices. At the same time, an always broader set of materials must be considered in the chemical synthesis and fabrication processes.

Manuscript received June 15, 2012; revised March 9, 2013; accepted April 16, 2013. Date of publication May 27, 2013; date of current version June 14, 2013. This work was supported in part by EC 7FP through Project GRADE under Contract 317839, by Project GO-NEXTs under Contract 309201, by Project GRAND under Contract 215752, and by the "Modeling and simulation of graphene nanoribbon FETs for high-performance and low-power logic applications" (MIUR-PRIN) Project (Prot. 2008S2CLJ9).

The authors are with the Dipartimento di Ingegneria dell'Informazione, Università di Pisa, Pisa I-56122, Italy (e-mail: gfiori@mercurio.iet.unipi.it; g.iannaccone@unipi.it).

Digital Object Identifier: 10.1109/JPROC.2013.2259451

In this context, materials and device modeling capabilities are an outstanding asset to perform timely and low-cost exploration of materials and technology options. They can really enable to early select the most promising routes for experimental investigation and for prototype fabrication.

Multiphysics and multiscale (MS) approaches are gaining relevance, because they offer a compelling tradeoff between physical accuracy and computational efficiency, and the possibility to adaptively tailor the level of accuracy to the simulation at hand.

MS approaches have another intrinsic advantage, since they enable one to choose the most appropriate hierarchy of physical descriptions (single atoms, solid-state materials, devices, and circuits) for each functional block of the device or system, through the definition of local *interfaces* for information exchange between different physical abstraction levels.

As has been observed in a recent document presenting the consensus of the computational nanoelectronics community [1]: "Multiscale modeling is capable of bridging across the different length scales. The concept is based on the observation that not all interactions must necessarily be treated within the first-principles framework. In an ensemble of small systems, certain variables average out and can be replaced by mean characteristic values which enter as parameters into the next level."

We should also notice that this extreme flexibility is inextricably linked to the great challenge of MS approaches: generalize the simulation workflow, which at present requires one to define *ad hoc* level hierarchies and information exchange interfaces for each simulated system.

Several examples of MS approaches to nanotechnology, and in particular to graphene nanoelectronics, have appeared in recent years. This is also facilitated by the very simple chemical properties of carbon that allows quantum chemistry tools to be used for relatively large structures. Almost all approaches are based on the present availability of very sophisticated *ab initio* quantum chemistry codes, such as VASP [2], AB-INIT [3], ONETEP [4], SIESTA [5], QUANTUM ESPRESSO [6], that often implement linear scaling approaches enabling the simulation of large molecules, especially in parallel computing clusters. Present day MS simulation projects are typically focused on how to build on existing *ab initio* tools, and in defining clear-cut or—when possible—quasi-automatic paths across different physical descriptions, in order to achieve results with the detail most appropriate for the system under investigation. We discuss in the following sections recent attempts to cover all physical levels of abstraction, from *ab initio* (i.e., the most fundamental description) to compact modeling for circuit performance evaluation.

The rest of the paper is organized as follows. In Section II, we present the issues related to modeling of graphene-based electron devices at different physical scales with special focus on materials. In Section III, we discuss the electronic and transport properties of graphene-based materials such as energy dispersion relation and mobility. In Section IV, we shift to the device level, focusing on the performance of graphene-based transistors based on different structures and operating principles, highlighting how *ab initio* simulations can be used to extract information needed to perform assessment of transistor operation and performance. Finally, we draw our conclusion.

II. MODELING AT DIFFERENT LEVELS OF ABSTRACTION

Understanding the potential of a new material for electronic applications requires a thorough assessment of its properties, including microscopic physical characteristics (e.g., the complete band structure, defects, structural properties), electrical properties (mobility, interband tunneling, quantum capacitance) and device performance figures (e.g., current drive, leakage currents, cutoff frequency). To this purpose, proper methods and approaches must be selected according to a criterion of best tradeoff between accuracy and computational cost.

In this section, we review the main simulation approaches, spanning from *ab initio* methods able to capture the relevant physics at the atomic level, up to analytical models required to investigate transistor performance in integrated circuits. We will also highlight the interfaces between the different levels of abstraction, i.e., the information that must be exchanged between adjacent levels.

A. *Ab Initio* Modeling

Ab initio calculations are the method of choice to understand the basic properties of a new or chemically modified material. With the aim of performing MS simulations, *ab initio* methods can provide fundamental quantities such as energy dispersion relations (from which effective masses and energy gaps can be extracted), metal work functions, electron affinities, and scattering rates. Density functional theory (DFT) has become a popular approach in the semiconductor and molecular device simulation community, since it deals with one-body electron density rather than with many-particle wave functions, as other variational methods.

DFT originates from the work of Hohenberg *et al.* [7], [8]. The Hohenberg and Kohn theorem states that—taken a system of N particles—there is a one-to-one correspondence between density in the ground state $n(\mathbf{r})$ and the external potential acting on it. This means not only that given the external potential, and, hence, the Hamiltonian, the electron density is uniquely determined, but that also the inverse is true, i.e., given the electron density, we can uniquely determine the external

potential. In other words, we can find a functional F so that

$$V_{\text{ext}} = F[n(\mathbf{r})]. \quad (1)$$

The Kohn–Sham equation reads

$$\left[-\frac{\hbar^2}{2m_0}\nabla^2 + U_L(\mathbf{r}) + V_H(\mathbf{r}) + V_{\text{exc}}(\mathbf{r})\right]\psi_i(\mathbf{r}) = \epsilon_i\psi_i(\mathbf{r}) \quad (2)$$

where

$$V_{\text{exc}} = \frac{\partial E_{\text{exc}}[n]}{\partial n(\mathbf{r})} \quad (3)$$

E_{exc} is the exchange-correlation functional, U_L is the lattice potential, V_H is the Hartree potential, and ε_i are the Lagrange multipliers needed to minimize (2).

The exact functional for the exchange correlation is not known *a priori*, therefore different assumptions can be done. The most common one is the local density approximation (LDA) [8] (or its extension to spin, i.e., local spin density approximation (LSDA) [9]), where the functional depends on the electronic density as a function of position, and the generalized gradient approximation (GGA) [10], where also the gradient of the density is taken into account.

DFT calculations work well in predicting the structure and the thermodynamic properties of solids and molecules, as well as the density of states [11]. On the other hand, DFT fails to accurately compute the barriers of chemical reactions, the energies of dissociating molecular ions, and charge transfer excitation energies.

DFT also overestimates the binding energies of charge transfer complexes and the response to an electric field in molecules and materials. For what concerns the computation of the energy bandgap, which is critical for device performance, DFT calculations clearly underestimate experimental results. Just to cite one example, DFT–LDA gives a bandgap in Silicon equal to 0.47 eV, while experiments have shown that bandgap is equal to 1.17 eV at room temperature [12].

If energy gap or energy barriers are the quantity of interest, the GW approximation [13] is more accurate. In the GW approximation, within the Green's function formalism, the Schrödinger equation can be expressed as

$$\left[-\frac{\hbar^2}{2m_0}\nabla^2 + U_L(\mathbf{r}) + V_H(\mathbf{r})\right]\psi_i(\mathbf{r}) + \int d\mathbf{r}'\Sigma(\mathbf{r},\mathbf{r}')\psi_i(\mathbf{r}') = \epsilon_i\psi_i(\mathbf{r}). \quad (4)$$

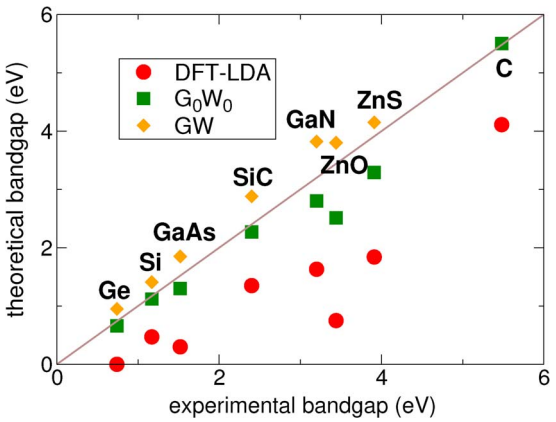

Fig. 1. ***Experimental and theoretical bandgap energy of different materials. Values have been extracted from [12].***

$\Sigma(\mathbf{r},\mathbf{r}')$ is the so-called self-energy and can be computed as suggested in [13] as

$$\Sigma = iGW \quad (5)$$

where G is the Green's function of the many-body system, and W is a function taking into account the screened Coulomb interaction.

Equation (5) gives the name to the GW approximation and is solved through a self-consistent iterative scheme. Good results can, however, be achieved already at the first iteration, i.e., the so-called G_0W_0 approximation [14].

In Fig. 1, experimental and theoretical bandgaps obtained through DFT, GW, and G_0W_0 approximations for different materials are compared [12]. It is apparent that GW provides more accurate bandgaps than DFT–LDA simulations, with a slight overestimation of the experimental results.

B. Atomistic Modeling

Ab initio calculations can provide accurate information on the electronic properties with high cost in terms of computing time. From a computational point of view, DFT complexity increases as N^3, where N is the total number of considered orbitals. As a consequence, investigation of systems larger than few hundred atoms can be prohibitive.

Larger systems can be studied with an alternative way to define the Hamiltonian of the material under investigation on an atomistic basis set, by means of a set of fitting parameters that manage to reproduce the same dispersion relation as DFT calculations. This allows to efficiently compute electronic and transport properties, such as transmission coefficients and local density of states, of larger systems.

Extended Hückel theory (EHT) [15] can represent a viable option. In particular, the Hamiltonian is expressed

by means of a nonorthogonal basis set $\phi(\mathbf{r_i})$, and the Hamiltonian element of index (i, j) can be expressed as [16]

$$H_{i,i} = E_{i,i} \tag{6}$$

$$H_{i,j} = 0.5KS_{i,j}(H_{i,i} + H_{j,j}) \tag{7}$$

$$S_{i,j} = \int d^3\mathbf{r}\phi_i^*(\mathbf{r})\phi_j^*(\mathbf{r}) \tag{8}$$

where $E_{i,i}$ and K are fitting parameters, which depend on the material. In particular, generally $K = 1.75$ for molecules and $K = 2.3$ for solids [16].

The Hamiltonian can also be described through a semiempirical Slater–Koster tight-binding (TB) scheme [17], which generally requires a reduced number of orbitals as compared to EHT, with a decrease of the overall simulation wall time, at the expense of larger efforts in order to find the suitable Hamiltonian elements. Indeed, while in the EHT model, the Hamiltonian is univocally defined given the material and the atoms position, the elements of the TB Hamiltonians are essentially fitting parameters, and are to be selected *ad hoc*, especially when the material to be investigated presents defects, heterojunctions, or other kind of nonidealities.

Once the Hamiltonian is known, carrier transport and charge in correspondence of each atom can be computed by means of the nonequilibrium Green's function formalism [18].

The Green's function can be expressed as

$$G(E) = [EI - H - \Sigma_S - \Sigma_D - \Sigma_{ph}]^{-1} \tag{9}$$

where E is the energy, I is the identity matrix, H is the Hamiltonian of the material, and Σ_S and Σ_D are the self-energies of the left and right contacts, respectively. Nonelastic scattering can also be taken into account by defining a proper self-energy Σ_{ph} (Fig. 2).

If we assume that the chemical potentials of the reservoirs at the left and right channel ends are aligned at the equilibrium with the Fermi level of the material, the electron concentration is given by

$$n(\vec{r}) = 2\int_{E_i}^{+\infty} dE\left[|\psi_S(E,\vec{r})|^2 f(E - E_{F_S}) + |\psi_D(E,\vec{r})|^2 f(E - E_{F_D})\right] \tag{10}$$

while the hole concentration is

$$p(\vec{r}) = 2\int_{-\infty}^{E_i} dE\left\{|\psi_S(E,\vec{r})|^2[1 - f(E - E_{F_S})] + |\psi_D(E,\vec{r})|^2[1 - f(E - E_{F_D})]\right\} \tag{11}$$

where $\vec{r}$ is the coordinate of the carbon site, f is the Fermi–Dirac occupation factor, $|\psi_S|^2$ ($|\psi_D|^2$) is the probability that states injected by the left (right) contact reach the atom site ($\vec{r}$), and E_{F_S} (E_{F_D}) is the Fermi level of the left (right) reservoir.

The current can be computed as

$$I = \frac{2q}{h}\int_{-\infty}^{+\infty} dE\mathcal{T}(E)[f(E - E_{F_S}) - f(E - E_{F_D})] \tag{12}$$

where q is the electron charge, h is Planck's constant, and $\mathcal{T}(E)$ is the transmission coefficient computed as [18]

$$\mathcal{T} = -\mathrm{Tr}\left[\left(\Sigma_S - \Sigma_S^\dagger\right)G\left(\Sigma_D - \Sigma_D^\dagger\right)G^\dagger\right] \tag{13}$$

where Tr is the trace operator.

From a numerical point of view, the fastest method to invert (9) is represented by the recursive Green's function (RGF) technique [19], [20]. Attention must be paid to the determination of the self-energy matrix, which can be computationally demanding. In order to achieve fast results, one can rely on the method suggested by Sancho *et al.* [21], which results to be faster than a simple under-relaxation method. If instead the structure is periodic along the transport direction, the fastest method developed so far has been described by Luisier *et al.* [22], able to obtain the self-energy by means of a closed-form expression.

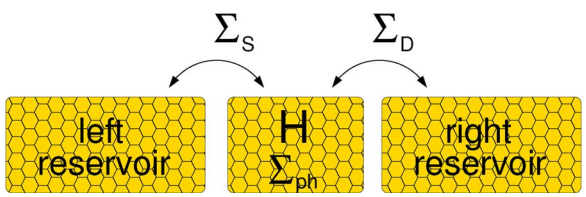

Fig. 2. *The NEGF approach: The device is univocally defined by the Hamiltonian H, which is connected to semi-infinite leads on the right and on the left by the self-energies Σ_S and Σ_D. Optionally, electron–phonon scattering can be considered through the definition of the self-energy Σ_{ph}.*

C. Semiclassical Device Modeling

Modeling tools of semiconductor devices routinely used in industry are based on a semiclassical physical description in the continuum of device structure and

transport. At this level of abstraction, the aim is to perform transport simulation of the entire device in order to compute the current-voltage and charge-voltage characteristics, using the parameters extracted through calibration with experiments or by means of accurate *ab initio*/atomistic simulations. Semiclassical device modeling is based on the coupled solution of an *electrostatics (i.e., Poisson) equation*, in which the potential profile is obtained considering charge densities as source terms, and a *transport equation* per type of charge carrier, in which charge densities are computed considering a known potential profile. The transport equation is typically based either on the drift-diffusion model, in which (low-field or field-dependent) mobility is the fundamental physical parameter, or on the Boltzmann transport equation, for which the scattering rates in the wave vector space are key parameters.

Semiclassical device modeling in the case of mundane semiconductor devices is extremely well documented and is already a mini industry, therefore we will direct the reader to textbook sources [23], [24]. Here, we want to discuss in more detail what is needed to simulate graphene-based devices at this level of physical description, and to mention some of the most interesting results obtained.

The information needed at this level of abstraction consists essentially of the following.

- *Band structure*: In the simplest possible case, one is just interested in the density of states. In the case of graphene-based materials, the parabolic approximation is typically applicable only for a small energy range (and not at all for 2-D graphene). The density of states can be directly computed by integrating a reasonable analytic approximation of the energy dispersion relation, as, for example, is discussed in Section III-C for bilayer graphene. At the other end of the spectrum, full bands can be used for a Monte Carlo solution of the Boltzmann transport equation (BTE).
- *Scattering rates*: Rates for the main scattering mechanisms, and in particular phonons, are required both for Monte Carlo solvers and for the computation of low- and high-field mobility to be used in the drift-diffusion model. We should stress the fact that the accurate computation of scattering rates in graphene-based materials is an active research field. Experiments are of little help as of now in determining scattering rates, since fabrication technology is still not mature enough to provide reproducible and controllable results, therefore computed scattering rates are more practical.
- *Interband tunneling rates*: Given the very small gap of graphene-based materials, interband tunneling cannot be neglected if one aims to obtain just qualitatively meaningful results. In both drift-diffusion and Monte Carlo modeling, interband tunneling probabilities can be translated in terms of rates of generation–recombination processes, which are well known and commonly treated in the context of semiclassical device modeling.

The computation of phonon scattering rates and low-field mobility in 2-D graphene has been performed in [25] through density functional perturbation theory, or on the basis of Su–Schrieffer–Heeger mode in [26]. Such results can be useful to calibrate simpler expressions for scattering rates based on the deformation potential approximations, for use in Monte Carlo device simulators, as, for example, in [27]. They are also useful to tune parameters to be used in descriptions at a higher level of abstraction, such as semiempirical Hamiltonians, in order to compute scattering rates and mobility in more complex structures, for example, an accurate computation of phonon-limited mobility in narrow graphene ribbons (nanoribbons) both at low fields [28]–[30] and at high-field, by means of a Monte Carlo solution of the single-particle BTE [31]. Still at this level, it has been possible to demonstrate the strong suppression of phonon-limited mobility as the width of nanoribbons is reduced in order to induce a significant energy gap. As shown in Fig. 3, suspended nanoribbons of width 1 nm, corresponding to an energy gap of order 1 eV, exhibit low-field mobility smaller than 500 cm^2/Vs, similar to mundane semiconductors.

The same scattering rates used to compute low-field mobility can be used in a Monte Carlo solver of the BTE, to compute high-field mobility and velocity saturation as a function of the longitudinal electric field. In [31], this has allowed to predict a peak of drift velocity and, therefore, a negative differential mobility in nanoribbons for large electric field, illustrated in Fig. 4. This property has also been observed in zigzag CNTs, and is due to the combined effect of the quasi-linear dispersion relation and the energy dependence of emission rates of optical phonons.

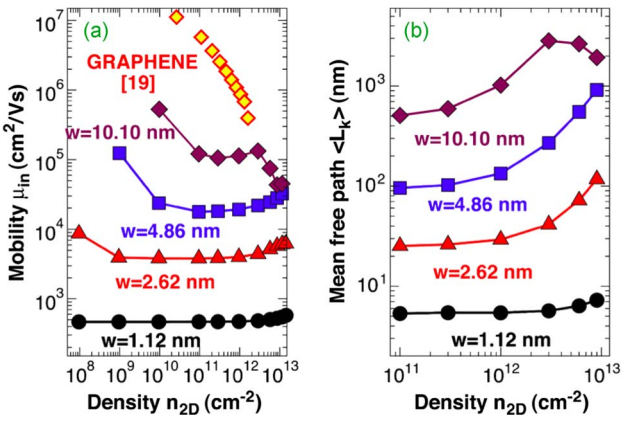

Fig. 3. ***Phonon-limited low-field mobility of suspended graphene nanoribbons as a function of 2-D electron density for different widths. From [30].***

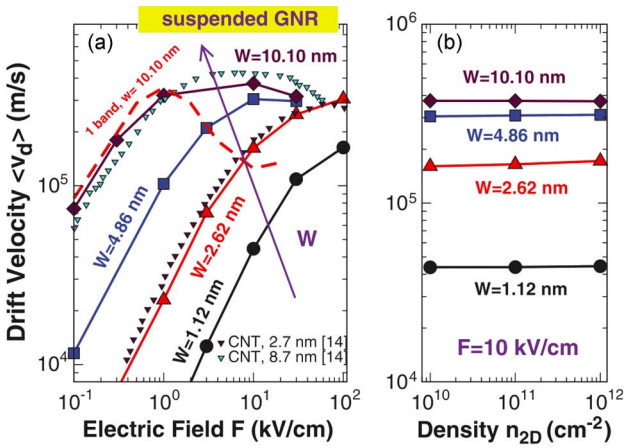

Fig. 4. *Drift velocity in graphene nanoribbons as a function of the longitudinal electric field for different nanoribbon widths. In all cases, electron density is 10^{12} cm^{-2}. Dotted lines are from the literature [32] for zigzag CNTs. The red dashed line is the very emphasized effect one would obtain with a model including a single 1-D subband. Figure from [31].*

The energy dispersion relation and mobility as a function of longitudinal electric field are key to device modeling based on the drift-diffusion transport model. The former is required to compute charge densities and interband tunneling rates as a function of the longitudinal electric field. In the case of graphene transistors, one has to couple 2-D drift-diffusion transport, given the planar nature of graphene, to 3-D electrostatics. In addition, one has to take into account both types of charge carriers, and interband tunneling in terms of generation–recombination processes, as in [33].

More detailed information, and, in particular, the full-band structure and scattering rates associated with different physical mechanisms (acoustic and optical phonons, remote phonons, impurities) can be used to perform device simulations with a 3-D semiclassical Monte Carlo solver [34]. In this case, the description is less accurate compared with an NEGF formalism, but the simulations can more directly include different scattering sources and time-dependent behavior.

Semiclassical device modeling is also the method of choice for very large (few micrometers) graphene transistors [35], [36]. In that case, the coupled poisson-drift-diffusion equations are the most appropriate, using mobility, generation–recombination rates, and density of states provided by more accurate simulations or experiments.

D. Analytical Modeling

Analytical models of graphene-based electron devices can provide useful insights to estimate device and circuit performance and to explore the design space, exploiting results from all other levels of abstraction previously described, and from experiments. Physicists and engineers must properly consider four different aspects in the analytical modeling of graphene-based transistors.

1) The peculiar band structure of monolayer graphene and of the many possible graphene-based channels that have been considered with the aim of circumventing the problem of the zero graphene gap, for example, graphene nanoribbons (GNRs), bilayer graphene, epitaxial graphene on SiC, lateral heterostructures.
2) A simplified model of transport in the channel, suitable for analytical description. For example, a ballistic or quasi-ballistic transport model, or a drift-diffusion model.
3) Electrostatics, simplified as to be mainly one dimensional, or suitable for description as a simple network of capacitances.
4) Tunneling currents, considering both Schottky barriers and interband tunneling.

Starting from the required ingredients listed above, analytical models are typically developed *ad hoc* for the specific device under investigation. Therefore, in the following, we prefer not to discuss analytical models in general terms, but to mention specific attempts to use analytical models in graphene device research, to let the reader appreciate the variety of available approaches.

For example, Zhao *et al.* proposed an analytical model of GNR FETs [37], including points 1–3 of the list above. Two-dimensional electrostatics was taken into account with a simple capacitive network, including quantum capacitances computed from the knowledge of GNR dispersion relation. Transport has been described with a top-of-the-barrier model considering a backscattering coefficient as suggested by Lundstrom *et al.* [38]. They could neglect interband tunneling because they considered a nanoribbon width that would provide an energy gap of 0.5 eV and a supply voltage of 0.5 V.

Similarly, Jimenez [39] considered a Schottky-barrier GNR FET. In the model, he had to include tunneling through Schottky barriers of both electrons and holes, assuming exponential barriers, and considered a simpler 1-D electrostatics. Scattering was assumed to occur only at the Schottky barriers and not in the channel.

Michetti *et al.* [40], [41] considered GNR FETs based on both ohmic contacts and Schottky barrier contacts, including a compact macromodel capable to describe in a seamless way the whole range of transport regimes ranging from fully ballistic to drift diffusion. The macromodel is based on describing a generic FET as a proper *chain* of n_b ballistic MOSFETs in series, where n_b is roughly the ratio of the channel length L to the mean free path λ. It can be further simplified into the series of two transistors with common gate: a drift-diffusion transistor of length $(L-\lambda)$ at the source side and a ballistic transistor at the drain side.

In case Schottky barriers are present at both the source and the drain, as shown in Fig. 5, the macromodel

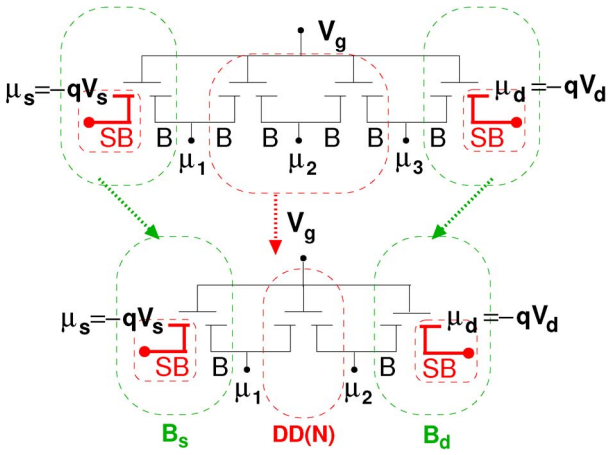

Fig. 5. *Chain of n_b ballistic FETs with Schottky barrier contacts at the source and drain (first and last contacts). The chain of ballistic transistors can be described as the series made by a central drift-diffusion transistor of channel length $L-\lambda$ section accounting for dissipative transport in the N-2 internal nodes and by head and tail ballistic transistors accounting for the Schottky barrier contacts with source and drain. From [41].*

has three transistors in series: a ballistic FET with Schottky barrier at the source, a drift-diffusion transistor of length $(L-2\lambda)$ in the middle, and another ballistic FET with Schottky barrier of the source. This model has been demonstrated to be accurate for 1-D dissipative transistors [41]. The same approach was demonstrated to be robust and rigorous for 2-D transistors in the case of nondegenerate and degenerate electron gas [42], [43].

In the case of 2-D graphene-based transistors, Wang *et al.* [44] proposed a compact virtual-source model of graphene-based FETs including mobility saturation, access resistance, and simplified 1-D electrostatics. Let us stress the fact that access resistance is a critical aspect and one of the main performance limitations of graphene-based electron devices. In order to model access resistance in a proper way, one must take into account its dependence on the carrier density in the access regions and near the contacts, which in turn depend on the back gate or substrate bias.

Several analytical models for graphene transistors have focused on bilayer graphene, which can have a small gap, and epitaxial graphene on SiC, which arguably could have a small gap [45]. Ryzhii *et al.* [46] have proposed an analytical model for bilayer graphene FETs, including gap dependence on the gate voltage (discussed in some detail in Section III-C), and both ballistic and dissipative transport. However, they completely discarded band-to-band tunneling, and the effect of electrostatic screening of the two graphene monolayers. Such aspects have been properly taken into account by Cheli *et al.* [47], with a restricted focus on ballistic transport.

Band-to-band tunneling is extremely limiting in bilayer graphene devices, because the attainable energy gap is close to 0.1–0.2 eV, therefore much smaller than the minimum supply voltage for a conventional FET at room temperature (0.4–0.5 V). Given the small tunneling effective mass of bilayer graphene, this translates into high leakage when the device is in the OFF-state. The effect of electrostatic screening goes in the same direction, since the potential difference between the two layers is reduced by screening, and hence the induced band gap.

Similar analysis has been made for the case of epitaxial graphene on SiC including both ballistic and dissipative transport in standard FETs [48], and in tunnel FETs [49]. Both works assume a gap 0.24 eV induced by the interaction between graphene and the SiC substrate, as observed in a 2008 experiment [45]. However, we must warn the reader that subsequent experimental works exhibited smaller or negligible bandgaps [50] and that the issue is still debated.

III. ELECTRONIC AND TRANSPORT PROPERTIES OF GRAPHENE-BASED MATERIALS

Understanding the electronic and transport properties of graphene-based materials is essential to assess transistor performance. From an engineering point of view, the most relevant quantities are represented by the effective mass, the bandgap, the electron affinity (all can be derived from energy dispersion relation), and by the mobility.

Graphene lacks a fundamental property of materials for electronic applications: the bandgap. In order to tackle this problem, different solutions have been proposed in the past, such as GNRs, bilayer graphene (BG), or functionalized graphene, which are the focus of the following sections.

A. Graphene Nanoribbon

Cutting 2-D graphene in narrow stripes leads to lateral confinement, which induces a bandgap. Depending on whether graphene is cut along the *x*- or *y*-directions [Fig. 6(a)], the energy dispersion relations and the electrical properties change. In particular, if transport is along the *y*-direction, we refer to zigzag GNRs, otherwise to armchair GNRs.

Modeling the edges is an important aspect to be taken into account in order to obtain accurate energy dispersion relations. As shown in [51]–[53] through *ab initio* calculations, the energy bandgap shows an oscillating behavior as a function of the width, with average roughly proportional to the inverse of the width. This is due to energy relaxation at the edges, which plays a very important role in inhibiting the existence of fully metallic nanoribbons. Such behavior is in agreement with experimental results [54] and cannot be reproduced if one

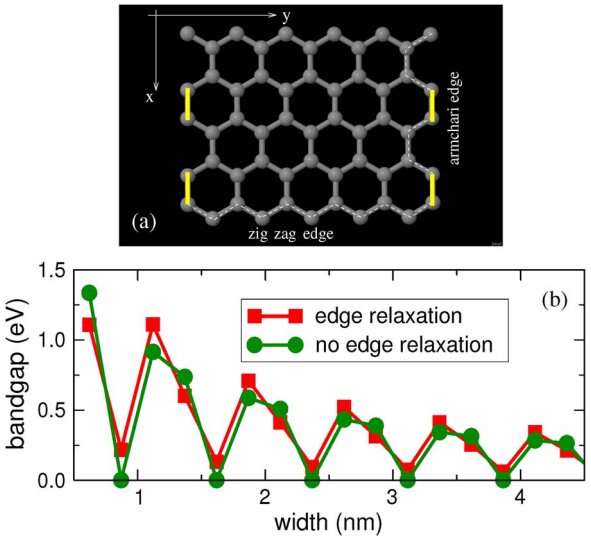

Fig. 6. *(a) Graphene lattice, where zigzag and armchair edges have been highlighted. (b) Energy bandgap for an armchair GNR as a function of GNR width, both when considering or not edge relaxation.*

does not consider edge effects [55], [56]. In Fig. 6(b), we show the bandgap for an armchair GNR as a function of width. As can be noted, metallic behavior appears when edge relaxation is not considered, while semiconducting behavior appears if one takes into account energy relaxation at the borders.

From a numerical point of view, this translates in modifying the tight-binding Hamiltonian in [56], by multiplying the hopping parameters between the atoms highlighted in yellow in Fig. 6(a) by a factor 1.12. In this way, it is possible to obtain a tight-binding description of the energy dispersion relation, which is in good agreement with *ab initio* results.

A simple analytical expression for the energy bandgap in armchair GNR has been derived in [51]. If N is the number of dimer lines, which can be expressed as a function of an integer p, i.e., $N = 3p$, $N = 3p+1$, or $N = 3p+2$, we obtain three bandgap (E_G) families

$$E_{G_{3p}} = E^0_{G_{3p}} - \frac{8|\delta t_{CC}|}{3p+1}\sin^2\left(\frac{p\pi}{3p+1}\right) \tag{14}$$

$$E_{G_{3p+1}} = E^0_{G_{3p+1}} + \frac{8|\delta t_{CC}|}{3p+2}\sin^2\left[\frac{(p+1)\pi}{3p+2}\right] \tag{15}$$

$$E_{G_{3p+2}} = E^0_{G_{3p+2}} + \frac{2|\delta t_{CC}|}{p+1} \tag{16}$$

where $\delta = 1.12$, t_{CC} is the carbon–carbon hopping parameter generally taken equal to -2.7 eV, and the bandgaps computed for the GNR without considering energy relaxations are

$$E^0_{G_{3p}} = |t_{CC}|\left[4\cos\left(\frac{p\pi}{3p+1}\right) - 2\right] \tag{17}$$

$$E^0_{G_{3p+1}} = |t_{CC}|\left\{2 - 4\cos\left[\frac{(p+1)\pi}{3p+2}\right]\right\} \tag{18}$$

$$E_{G_{3p+2}} = 0. \tag{19}$$

The extracted effective mass m_j on the jth subband reads instead [41]

$$m_j = -\frac{2}{3}\frac{\hbar^2 E_{Cj0}}{a^2 t_{CC}^2 A_j} \tag{20}$$

where $A_j = \cos(\pi j/(N+1))$. For the first conduction subband $E_{Cj0} = E_G/2$ and j (which runs from 1 to l) is the index for which A_j is closest to $-1/2$.

High mobility is the single most important aspect that makes graphene interesting for nanoscale electronics. It is, therefore, of paramount importance to understand if also nanostructured graphene can preserve the high mobility. For GNRs, few interesting experiments are reported in [57] and [58], but the many different scattering mechanisms present at once in the measured samples make it difficult to provide an exhaustive interpretation of the single physical mechanisms limiting mobility. From this perspective, theoretical investigations can assess the relative impact of different sources of nonidealities on mobility and provide realistic evaluation of the perspectives of graphene in nanoelectronics.

The impact of edge roughness, epoxide adsorbates and doping atoms like boron and nitrogen in the overall conductance of GNRs have been investigated by means of an MS approach in [59]–[61], respectively. In particular, the fundamental physics at the atomic scale has been captured by using *ab initio* simulations on a limited portion of the GNR including nonidealities, and then extracting the main parameters (i.e., charge, potential distribution, or energy dispersion relations). Such parameters have been then fitted with a tight-binding Hamiltonian in order to compute the conductance in a system containing thousands of atoms. Simulations have shown that when applying a small potential difference between the contacts at GNR ends, the ambipolar behavior can be suppressed, inducing a so-called mobility gap.

A comprehensive analysis of intrinsic mobility limited by single vacancy defects, ionized impurities, edge roughness, and electron–phonon interaction has been performed in [62], where a statistical investigation of the different sources of nonidealities has been performed

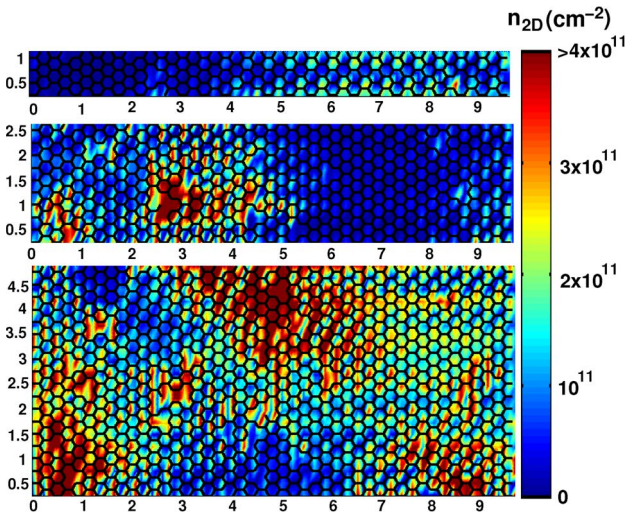

Fig. 7. *Carrier density n_{2D} in the GNR channel for different GNR widths. (From top to bottom) $W = 1.12$, 2.62, and 4.86 nm. Figure taken from [62].*

within the tight-binding approach, using parameters extracted from *ab initio* calculations [51] and EHT [63].

The presence of single vacancy defects leads, for example, to a strong Anderson localization [64], degrading electron mobility and creating percolating paths in wider GNRs, while fully blocking conduction in the narrower ones (Fig. 7).

The total mobility computed with Mathiessen's rule is shown in Fig. 8 and compared with experimental data available in [57]. As can be seen, when using parameters in [65] for electron–phonon coupling, line edge roughness is the most limiting mechanism for very narrower GNRs, while for wider GNRs defect scattering is predominant, if a concentration of 0.5% vacancies per carbon atom is considered. As observed in [62], the same conclusion holds even when considering much lower deformation potentials for phonons that decrease the impact of phonon scattering, such as those computed in [25] through *ab initio* simulations.

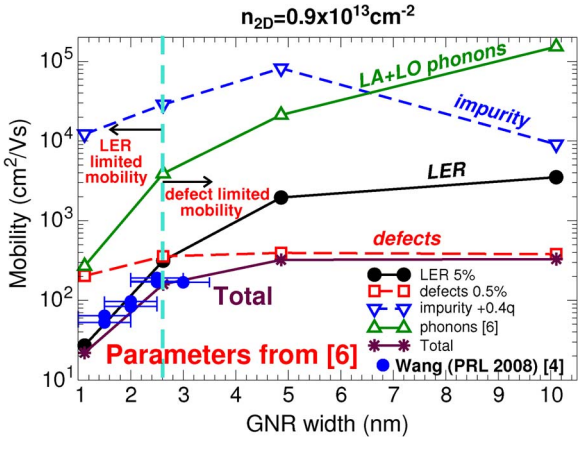

Fig. 8. *Mobility limited by phonons, LER, defect and impurity scattering in the inversion regime for a line edge roughness of 5%, and defect concentration of 0.5%. The parameters for the scattering rates have been taken from [65]. The experimental mobility from [57] is also reported. $n_{2D} = 0.9 \times 10^{13}$ cm^{-2}, $n_{IMP} = 10^{12}$ cm^{-2}. Figure from [62].*

B. Functionalized graphene

Chemical functionalization of graphene has been first demonstrated by Elias *et al.* [66] as a technological solution in order to engineer the bandgap in graphene-based materials [66].

Sofo *et al.* [67] first predicted stability of 100% hydrogenated graphene through standard DFT calculations with a GGA. More detailed simulations have been performed in [68], where GW simulations have shown energy bandgaps larger than 2 eV, as compared to previous results based on DFT simulations in [67] and [69] (i.e., GW bandgap equal to 5.4 and 4.9 eV, respectively).

Fluorine has been taken into account in [70], demonstrating a clear dependence of the energy gap on fluorine concentration, as well as on lithium [71].

A performance assessment of transistors based on functionalized graphene requires the computation of transport along the channel. To make computation efficient, a tight-binding Hamiltonian is required. For example, an sp^3 Hamiltonian with three nearest neighbors has been computed in [72] by means of a least mean square fitting procedure, fitting the energy dispersion along the ΓM and ΓK directions obtained with the GW approximation. Particular attention has been paid to the minimum and the maximum of the conduction and valence band edges, respectively, since those states contribute to transport the most. As can be seen in Fig. 9, the adopted procedure manages to reproduce the GW bands and provide a better fitting than a simple nearest neighbor approach.

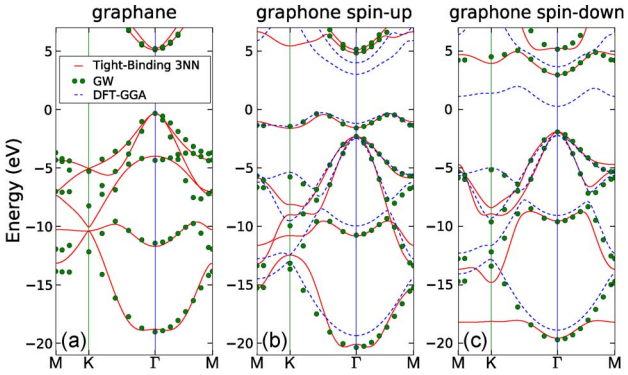

Fig. 9. *Energy bands computed for (a) 100% and (b)–(c) 50% hydrogenated graphene, using tight-binding three nearest neighbor (solid line), GW (dots), and DFT–GGA approaches (dashed lines). In the case of 50% (b) spin-up and (c) spin-down bands are shown. Figure from [72].*

Mobility in 2-D hydrogenated and fluorinated graphene at different percentages has been studied in [73] with an MS approach. In particular, the deformation potential has been computed following the Bardeen and Shockley's [74] approach and relating the band-edge shift to the differential displacement of the crystal by the electron–phonon coupling Hamiltonian as in [75] and [76].

In particular, for nondegenerate bands [77], the band edge shift $\delta E(k)$ due to acoustic phonon is related to the fractional volume change of the elementary cell $\delta V/V_0$ by the equation

$$\delta E(k) = E_1\left(\frac{\delta V}{V_0}\right) \tag{21}$$

where E_1 is the so-called deformation potential. Once E_1 is known, carrier mobility can be estimated by means of the Takagi formula [78], which reads

$$\mu = \frac{e\hbar^3\rho S_l^2}{k_B T m_e m_d E_1^2} \tag{22}$$

where ρ is the mass density, T is the temperature, k_B is Boltzmann's constant, e is the elementary charge, S_l is the sound velocity, m_e is the mass along the transport direction, and m_d is the equivalent density-of-state mass defined as $m_d = \sqrt{m_x m_y}$. S_l, m_e, and m_d are computed by means of *ab initio* calculations, and are extracted from the phonon $\omega(k)$ and electronic dispersion relations $E(k)$, according to $S_l = [\partial\omega(k)/\partial k]$ and $m_e = \hbar[\partial^2 E(k)/\partial k^2]^{-1}$. The deformation potentials E_1 are instead computed through mimicking the lattice deformation due to phonons by multiplying the lattice constant by different factors, i.e., dilating and relaxing the primitive cell. E_1 is then obtained computing the energy shift of the bottom of the conduction band δE and applying (21).

The mobility obtained along the ΓK and ΓM directions is shown in Table 1.

The low mobility predicted for highly hydrogenated graphene is in quantitative agreement with available experimental data recently reported in the literature as a function of the exposure time to H [79]. While fluorinated compounds show the smallest mobilities among the considered structures, 50% and 25% hydrogenated graphene (H50% and H25%, respectively) exhibit mobilities comparable to bulk silicon.

Table 1 Electronic Mobility μ Taken From [73]. In the First Column, the Number After the Atomic Symbol (Either C or F) Refers to the Hydrogenation Percentage of the Graphene Flake

	$\mu_{\Gamma K}\left(\frac{cm^2}{V\,sec}\right)$	$\mu_{\Gamma M}\left(\frac{cm^2}{V\,sec}\right)$
H 100%	107.4	107.4
H 75%	73.0	78.7
H 50%	1058.0	1058.0
H 25%	703.5	3030.6
F 100%	42.5	42.5
F 50%	41.5	41.5

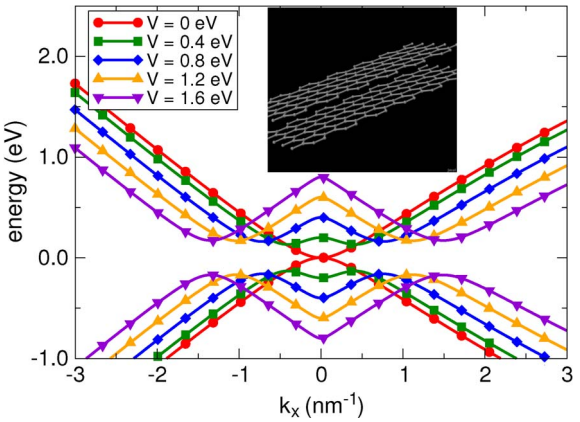

Fig. 10. *Energy bands in correspondence of the K point ($k_x = 2\pi/(3\sqrt{3}a_{CC})$ and $k_y = \pi/(3\sqrt{3}a_{CC})$) for different V, i.e., the difference between the potential at the top and bottom layers. In the inset, the bilayer graphene lattice.*

C. Bilayer Graphene

Bilayer graphene is composed by two graphene monolayer flakes stacked one over the other, as shown in the inset of Fig. 10. In particular, it has been theoretically demonstrated in [80] and [81] to possess an interesting electrical property, i.e., a bandgap tunable by means of an applied vertical electric field.

In Fig. 10, the energy dispersion relation in correspondence of the K point is shown for different V, the energy difference between the top and bottom layers.

For $V = 0$ eV, the bandgap is zero, and the energy dispersion is parabolic and no more linear as in 2-D graphene. The larger the V, the larger is the bandgap. In addition, the conduction (valence) band minimum (maximum) shifts from K as soon as V increases, leading to the so-called "Mexican-hat" behavior and to bandgap saturation of few hundreds meV as soon as V is larger than 0.4 eV.

Energy dispersion relations have been computed by means of *ab initio* simulations in [82], while a tight-binding Hamiltonian has been considered in [83] and [84]. In particular, the energy dispersion relation can be expressed as

$$E(\mathbf{k}) = \frac{V_1 + V_2}{2} \pm \sqrt{|f(\mathbf{k})|^2 + \frac{V^2}{4} + \frac{t_\perp^2}{2} \pm \frac{1}{2}\sqrt{4(V^2 + t_\perp^2)|f(\mathbf{k})|^2 + t_\perp^4}} \tag{23}$$

where V_1 and V_2 are the potential energies on the first and second layers, respectively, $V = V_1 - V_2$, $t_\perp = -0.35$ eV is the interlayer hopping parameter [84], and $\mathbf{k} = k_x\hat{k}_x + k_y\hat{k}_y$. $f(\mathbf{k})$ can instead be expressed as [85]

$$f(\mathbf{k}) = t_{CC}e^{ik_x a/2}\left[2\cos\left(\frac{k_y a\sqrt{3}}{2}\right) + e^{-i3k_x a/2}\right] \quad (24)$$

which is equal to the well-known off-diagonal element of the 2×2 graphene p_z-Hamiltonian, where $a = \sqrt{3}a_{CC}$.

In order to capture bands energy dispersion in semi-analytical model aiming at assessing bilayer graphene performance, it would be rather advisable to obtain an expression within the effective mass approximation (EMA). As shown in [84], in correspondence of K, the energy dispersion relation reads

$$E(\mathbf{k}) = \frac{E_{gap}}{2} + \frac{\hbar^2}{2m^*}(|\mathbf{k}| - k_{min})^2 + \frac{V_1 + V_2}{2} \quad (25)$$

where

$$m^* = \frac{|t_\perp|\left(V^2 + t_\perp^2\right)^{\frac{3}{2}}}{2V(V^2 + 2t_\perp^2)}\frac{\hbar^2}{v_F^2} \quad E_{gap} = \frac{|Vt_\perp|}{\sqrt{V^2 + t_\perp^2}} \quad (26)$$

$v_F = 3a|t_{CC}|/2$ is the Fermi velocity, $\hbar$ is the reduced Planck's constant, and

$$k_{min} = \sqrt{\frac{V^2 + 2t_\perp^2}{V^2 + t_\perp^2}}\frac{|V|}{2v_F}. \quad (27)$$

As can be observed from (26), m^* diverges for $V = 0$. On the other hand, as can be seen in Fig. 10, the dispersion relation for $V = 0$ eV is parabolic with a corresponding mass equal to 0.043 m_0. In particular, as demonstrated in [47], a simple expression for the effective mass reads

$$\frac{m^*}{m_0} = 0.09V + 0.043. \quad (28)$$

IV. ASSESSMENT OF PERFORMANCE OF GRAPHENE-BASED TRANSISTORS

Research on alternative materials to continue downscaling of semiconductor technology until the 15-year horizon of the International Technology Roadmap for Semiconductors [86] has led increased efforts in assessing whether it is possible to take advantage of the high mobility of graphene by using it as channel material in nanoscale transistors.

Here we focus on three different alternatives: graphene nanoribbon, 2-D graphene heterostructures, and graphene bilayer FET.

A. Graphene Nanoribbon Transistor

As outlined in the Section III, 2-D graphene is a zero gap material, with linear dispersion in correspondence of the Fermi energy. Energy gap can, however, be induced by means of several technological solutions, such as lateral confinement or functionalization.

An MS approach using tight-binding atomistic simulation of GNR–FET, and based on an accurate energy band description using results obtained in [51], has been proposed in [87], where large I_{on}/I_{off} ratios have been shown to be possible for narrow devices. In particular, if V_{DD} is the power supply, I_{DS}, V_{DS}, and V_{GS} are the drain-to-source current, drain-to-source voltage, and gate-to-source voltage, respectively, $I_{on} = I_{DS}$ for $V_{DS} = V_{DD}$ and $V_{GS} = V_{DD}$, while $I_{off} = I_{DS}$ for $V_{DS} = V_{DD}$ and $V_{GS} = 0$ V.

A detailed study of the role of the contacts (either ohmic or Schottky) has been performed in [88] through the NEGF formalism, where ohmic contacts have shown superior performance as compared to the Schottky contact nanoribbon FETs. Due to the reduced lateral dimensions, the role of the edges can play a relevant role in degrading device performance.

The effect of edge roughness (Fig. 11) has been, for example, investigated in [89], where a self-consistent simulation of the Poisson and transport equations has been performed showing that induced midgap states can degrade the ON- and OFF-currents. The effect of edge chemistry has been studied in [90], focusing on the mobility in GNRs, and exploiting combined *ab initio* and NEGF simulations.

In [37], a semianalytical model including the effect of bond relaxation, edge scattering through a third-nearest-neighbor Hamiltonian has been considered to compute

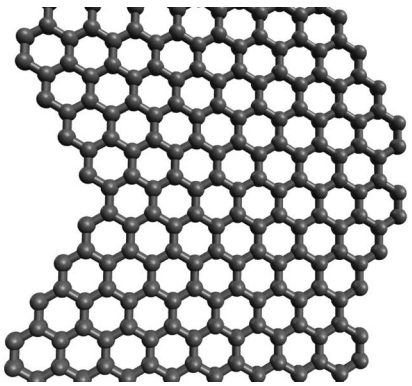

Fig. 11. *Example of edge roughness in a GNR.*

I–V characteristics in GNR–FETs as well as quantum capacitance for different channel widths.

All the aforementioned works agree in outlining that edge disorder is the main reason for performance degradation in narrow devices. In addition to that, it is very clear from Fig. 6 that a tolerance of just one atom in the nanoribbon width induced large changes in the gap, which in turn translates in a large variability of the I–V characteristics [87].

Since 2-D graphene has no gap but a very high mobility, it has been proposed as a suitable solution for radio-frequency (RF) applications, where the capability to switch the device off—which requires an energy gap of a fraction of eV—is not required.

Analytical models based on a accurate band description with a tight-binding Hamiltonian, and semiclassical top-of-the-barrier model for transport computation along the channel have been used in [35] and [91]–[93], to provide information on graphene-based transistors performance for RF applications, focusing on the saturation of the output characteristics experimentally observed [36]. The same issue has been addressed through more accurate Monte Carlo methods in [94] and NEGF formalism in graphene FETs [95] and GNRs [96], [97].

The main figures of merit for analog and RF performance of graphene-based transistors are the power gain and the so-called $f_{\max}$ frequency, i.e., the max frequency at which one can obtain power gain. It is important to consider that $f_{\max}$ increases with the transconductance, the output resistance, and the inverse of the contact resistance. While long channel devices still show a lightly pronounced saturation behavior, short channel devices output characteristics are completely linear, as demonstrated experimentally in [98]. From this perspective, bilayer graphene shows better performance, as demonstrated experimentally and theoretically in [99], while achieving voltage gain of roughly 35 and 10 in long- and short-channel devices, respectively. A recent theoretical comparison between FETs with bilayer and monolayer graphene channel shows higher output resistance and $f_{\max}$ in bilayer graphene FETs [100]. It is worth noticing that the so-called cutoff frequency f_T, often mentioned in the literature, is easier to measure but is less relevant for RF performance.

For what concerns digital applications, as already stated, 2-D graphene-based devices cannot comply with ITRS requirements. Some promising technological solutions have, however, been recently proposed and based on MS simulations, which will be described in detail in the Section IV-B and C.

B. Hexagonal Boron Carbon Nitride/Graphene Heterostructure Transistor

The current in the graphene-based transistor at the OFF-state is composed by two components [Fig. 12(a)]: the band-to-band tunneling current (red arrow), which represents the major contribution, and the thermionic component (green arrow), which is generally negligible.

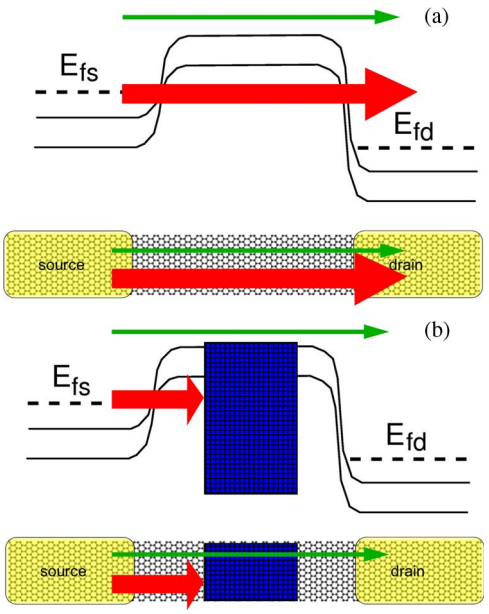

Fig. 12. *(a) Sketch of the band diagram of the device in the OFF-state, where both band-to-band tunneling (red arrow) and thermionic component of the current (green arrow) are depicted. (b) If a barrier is defined in the middle of the channel, only the thermionic component takes part to the current.*

In order to achieve good OFF-states, it would be advisable to reduce the tunneling component, while leaving unaltered the thermionic current.

To this purpose, in [101], a new device structure has been proposed based on a lateral heterostructure within the graphene channel (Fig. 12), which introduces a barrier capable to block the band-to-band tunneling component and the ambipolar behavior of the graphene FET. The requirements for the barrier material are that it has to be compatible with graphene technology, it has to possess a sufficiently large bandgap, and has to have sufficiently large mean free path for electrons.

One of the possible channel barrier materials proposed in [101] is hexagonal boron–carbon–nitride (hBCN), which exhibits almost perfect lattice match with graphene. The fabrication of hBCN/graphene heterostructure has been recently demonstrated [102]. Since the material is so new, an MS approach has been adopted to compute through *ab initio* calculations their main physical parameters (i.e., electron affinity, bandgap, barrier height seen by electrons and holes), which have then been exploited to define the tight-binding Hamiltonian needed to compute transport within the NEGF formalism.

The considered device structure is a double-gate FET with a channel consisting in a single-atomic-layer graphene/hBCN/graphene heterostructure, illustrated in Fig. 13. The hBCN region, of length t_B, is exactly below the

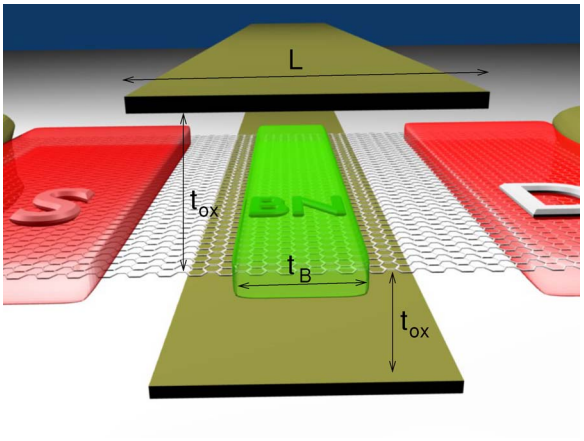

Fig. 13. *Illustration of the double-gate bilayer graphene TFET: the channel length is 40 nm, and n^+ and p^+ reservoirs are 40 nm long with molar fraction f. The device is embedded in 3-nm-thick SiO_2 dielectric. V_{top} and V_{bottom} are the voltages applied to the top and bottom gates, respectively.*

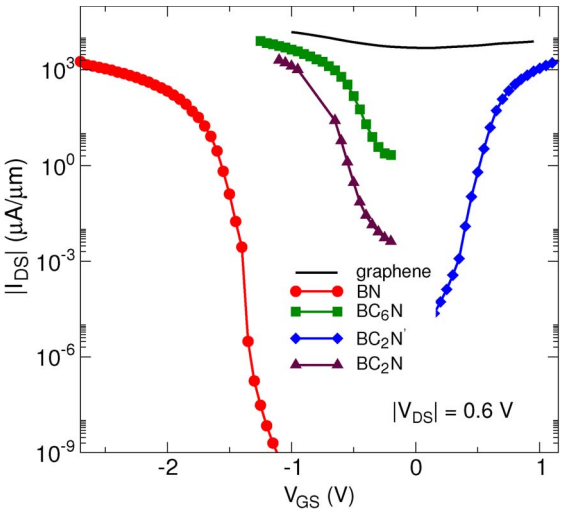

Fig. 14. *Transfer characteristics for the different barrier materials. All the considered devices are p-type except BC_2N', which is n-type. Molar fraction $|f| = 10^{-2}$ for BC_2N, BC_2N', and BC_6N, while $f = 5 \times 10^{-2}$ for BN. $t_B = 5$ nm. Taken from [101].*

gates, and acts as the barrier for carrier flow. Two metallic gates have a length $L > t_B$ and, therefore, overlap on the graphene regions, and are separated from the channel by a silicon oxide layer of thickness 1 nm. Graphene regions below the gate are undoped, whereas those forming the source and drain extensions are doped with donors or acceptors for obtaining nFETs or pFETs, respectively. The doping molar fraction f represents the number of doping atoms over the total number of carbon atoms in the contact extensions.

For the hBCN region, four different materials have been considered: boron nitride (BN), two different configurations with 50% concentration of carbon atoms (BC_2N and BC_2N', respectively) and 75% concentration of carbon atoms (BC_6N).

In Fig. 14, the transfer characteristics are shown for all the considered devices for $V_{DS} = 0.6$ V. Due to the large BN barrier height, BN devices have larger threshold voltage, and smaller I_{on}, but subthreshold swing (SS) similar to those obtained for the other devices.

In Table 2, the main figures of merit of FET performance are shown. As can be seen, BC_2N and BC_2N' FETs exhibit I_{on}/I_{off} larger than 10^4, meeting ITRS requirements.

This actually shows that hybridized graphene with intercalated carbon and hBCN represents an exceptional platform for exploring truly 2-D nanoelectronics. The possibility to engineer the electronic properties of the channel with hBCN allows to obtain high I_{on}/I_{off} graphene-based FETs.

C. Tunnel FET Bilayer Graphene Transistor

As discussed in Section III-C, applying a vertical field in bilayer graphene leads to a tunable bandgap. The largest attainable bandgap value is, however, of the order of $t_\perp$, i.e., the hopping parameter between two overlaying atoms belonging to different graphene layers, which is of the order of few hundred meV. As demonstrated in [103] through tight-binding simulations, such value is not sufficient to switch the channel off in bilayer graphene devices. The main problem is indeed the large band-to-band tunneling component in the OFF-states, which largely degrades performance in the subthreshold regime. Even an investigation in the parameter space through an analytical approach, validated against more accurate tight-binding simulations [47] has clearly demonstrated that such leakage cannot be effectively suppressed.

One, however, could think of turning this advantage into his own favor, fully exploiting band-to-band tunneling as in tunnel FET (TFETs).

Power consumption indeed represents today the most limiting factor in electronic system, so that technological solutions able to allow reduced power requirements are much needed. Reducing the supply voltage in digital electronic devices complies with these requirements.

Table 2 Channel Length (L), $I_{off}, I_{on}, I_{on}/I_{off}$ Ratio, Subthreshold Swing (SS)

Material	L (nm)	I_{off} $(\mu A/\mu m)$	I_{on} $(\mu A/\mu m)$	I_{on}/I_{off}	SS (mV/dec)
BC_2N	10	0.1	1736	17360	80
BC_2N	7	0.1	1600	16000	83
BC_6N	10	2.15	2143	996	116
BC_6N	7	2.55	2048	804	123
BC_2N'	10	0.1	1368	13678	66
BC_2N'	7	0.1	1285	12850	67
BN	10	0.1	491	4910	70

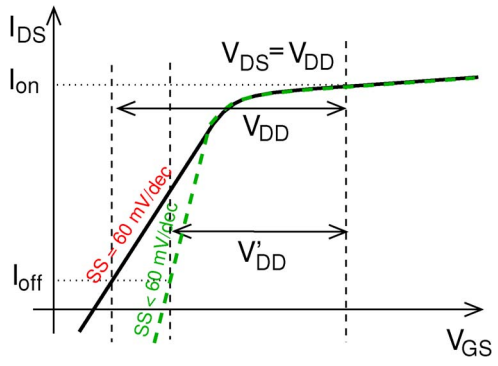

Fig. 15. *Transfer characteristics of a thermionic device with SS = 60 mV/dec (solid line) and tFET device with SS < 60 mV/dec (dashed line). TFET allows smaller power supply for the same I_{on}/I_{off} ratio as in thermionic device.*

However, the maximum attainable I_{on}/I_{off} ratio in thermionic devices is limited by the 60-mV/dec value for the SS.

Given the I_{on}/I_{off} ratio, power supply can only be strongly reduced if technological solution allowing SS < 60 mV/dec are provided as in the case of TFETs (Fig. 15).

TFETs based in bilayer graphene have been first proposed in [104]. The considered structure is shown in Fig. 16, and has been studied through an atomistic tight-binding Hamiltonian, exploiting parameters obtained by means of *ab initio* simulations [84].

A correct understanding of the band-to-band tunneling process is here of primary importance, so that atomistic simulations are the method of choice, since they are able to provide a quantitative estimation of such effects.

The device is a double-gate BG–TFET, with two gates one at the top and one at the bottom, driven by two independent gates, biased with V_{top} and V_{bottom}, respectively. The channel length L is 40 nm, as well as the source and drain reservoirs doped with molar fraction f. The SiO_2 dielectric is 3 nm thick.

Particular attention has to be posed to device band profile engineering. As shown in Fig. 16(a), where the band edge profile of the TFET in the OFF-state is depicted, the conduction and valence bands can be divided in five subregions along the transport direction: the source, the so-called virtual source, the channel, the virtual drain, and the drain. Deep in the source and drain regions, the conduction and the valence bands coincide because the vertical electric field rapidly goes to zero. A gap is induced in all the regions surrounded by the top and bottom gates, where a differential voltage $V_{diff} \equiv V_{top} - V_{bottom}$ is imposed, i.e., in the virtual source and drain regions and in the channel.

Six different carrier fluxes contribute to transport, identified with a letter in Fig. 16(a): tunneling electrons (A and B fluxes), tunneling holes (E and D fluxes), and thermally emitted electrons (C) and holes (F). In order to obtain a small I_{off}, all mentioned fluxes have to be minimized.

To this purpose, one can tune the bandgap by applying a proper vertical electric field (i.e., varying V_{diff}), or choosing the molar fraction of the reservoirs. The molar fraction of the source and drain leads indeed determines E_1 and E_2, the difference between the midgap potential in the channel (E_{ref}) and the midgap in the virtual drain and in the drain, respectively (same considerations obviously follow for the source): the higher f, the higher E_1 and E_2. Decreasing E_1 and E_2 can help in reducing E and D (or A and B in the source), but in turn increases thermionic emission (C and F).

In Fig. 16(b), the transfer characteristics as a function of V_{bottom} are shown when applying an ultralow supply voltage $V_{DD} = 0.1$ V, for different vertical electric field. As can be seen, the TFET can be perfectly switched off, with a steep subthreshold behavior and a large I_{on}/I_{off} ratio, as also reported in Table 3.

This opens the possibility of an exploitation of 2-D graphene for ultralow power digital applications.

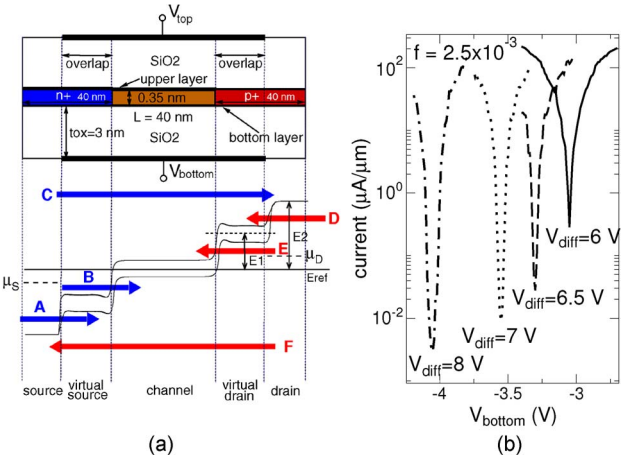

Fig. 16. *(a) Sketch of the double-gate bilayer graphene TFET: The channel length is 40 nm, and n^+ and p^+ reservoirs are 40 nm long with molar fraction f. The device is embedded in 3-nm-thick SiO_2 dielectric. V_{top} and V_{bottom} are the voltages applied to the top and bottom gates, respectively. Gate overlap has been also considered. Below, band edge profile of the device in the OFF-state. (b) Transfer characteristics of the double-gate BG–TFET for different V_{diff}. f is equal to 2.5×10^{-3} and $V_{DS} = 0.1$ V. Figure extracted from [104].*

Table 3 I_{on}/I_{off} Ratios, E_{gap} Computed in the Middle of the Channel, $\mathcal{E}$, the Electric Field in the Middle of the Channel, and Maximum Subthreshold Swing *SS* for Different V_{diff}

V_{diff} (V)	I_{on}/I_{off}	E_{gap} (eV)	$\mathcal{E}$ (MV/cm)	SS (mV/dec)
6	147	0.24	9.45	21
6.5	885	0.25	10.23	13
7	2822	0.260	11.02	12
8	4888	0.274	12.59	14

V. CONCLUSION

MS modeling of graphene nanoelectronics can enable a vision of nanotechnology in which materials are engineered at the atomic scale, and virtual nanofabrication laboratories are available for technology exploration, prototyping, and optimization. It is fair to say that we are still at the first stage of that vision: technology exploration.

Even at this stage of maturity, MS modeling provides a compelling advantage to theoreticians and experimentalists focusing on the basic properties of graphene, allowing them to test hypotheses in a qualitative and quantitative way, facilitating the design and refinement of actual experiments. It also provides a great advantage to technologists, by giving them the tools for an early assessment of the impact of the introduction of alternative—still poorly known—materials and structures.

We have shown that MS modeling is a powerful tool for exploring the possibilities to induce a gap in graphene-based materials, without an excessive degradation of mobility and reliability, and to test the basic electrical properties of materials and of device performance.

To conclude, we would like to briefly comment on three critical issues that need to be addressed in the medium term.

- Devise methodologies (either automatic or expert guided) to combine the simulation of specific building blocks at different levels of abstraction to model a complete complex device or a system. At the moment, we only have *ad hoc* solutions, and *ad hoc* physical information interfaces between different blocks. Once the community is able to move from *ad hoc* solutions to shared techniques, progress and scaling up to larger functional systems can proceed at a faster rate.
- Define specific test structures and methodologies for materials and devices to extract information useful for detailed MS modeling. This is extremely important because *ab initio* modeling will not be able to provide all the information needed within reasonable tradeoffs of accuracy and computing time. Again, progress is needed in this area, since this activity is not presently done in a systematic way.
- Further increase high-performance computing capabilities, in terms of 1) numerical methods, 2) availability of open-source codes to experiment and thinker with, and 3) parallel computing infrastructures. Indeed, more and more, MS simulations are based on advanced scripts combining open-source and proprietary simulations codes of different origin, running on high-performance or cloud-computing infrastructures.

Notwithstanding these challenges, MS simulations for graphene nanoelectronics—as for other new materials—have a chance to gradually move from being a research field to the status of a mainstream tool for technology development, as has already happened with computer-aided design for semiconductor technology. ■

REFERENCES

[1] F. Ortmann, S. Roche, J. C. Greer, G. Huhs, X. Oriols, T. Shulthess, T. Deutsch, P. Weinberger, M. Payne, J. M. Sellier, J. Sprekels, J. Weinbub, K. Rupp, D. Vasileska, E. Alfinito, L. Reggiani, D. Guerra, D. K. Ferry, M. Saraniti, S. M. Goodnick, A. Kloes, L. Colombo, K. Lilja, J. Mateos, T. Gonzalez, E. Velazquez, P. Palestri, A. Schenk, and M. Macucci, "Multi-scale modeling for devices and circuits," 2012.

[2] VASP. [Online]. Available: http://www.vasp.at

[3] AB-INIT. [Online]. Available: http://www.abinit.org

[4] ONETEP. [Online]. Available: http://www.onetep.org

[5] SIESTA. [Online]. Available: http://icmab.cat/leem/siesta

[6] QUANTUM ESPRESSO. [Online]. Available: http://www.quantum-espresso.org

[7] P. Hohenberg and W. Kohn, "Ihnomogeneous electron gas," *Phys. Rev.*, vol. 136, pp. B864–B871, 1964.

[8] W. Kohn and L. J. Sham, "Self consistent equations including exchange and correlation effects," *Phys. Rev.*, vol. 140, pp. A1133–A1138, 1965.

[9] S. H. Vosko, L. Wilk, and M. Nusair, "Accurate spin-dependent electron liquid correlation energies for local spin density calculations: A critical analysis," *Can. J. Phys.*, vol. 58, pp. 1200–1211, 1980.

[10] D. C. Langreth and J. P. Perdew, "Theory of nonuniform electronic systems I: Analysis of the gradient approximation and a generalization that works," *Phys. Rev. B*, vol. 21, pp. 5469–5493, 1980.

[11] A. J. Cohen, P. M. Sanchez, and W. Yang, "Insights into current limitations of density functional theory," *Science*, vol. 321, no. 5890, pp. 792–794, 2008.

[12] F. Tran and P. Blaha, "Accurate band gaps of semiconductors and insulators with a semilocal exchange-correlation potential," *Phys. Rev. Lett.*, vol. 102, 2009, 226401.

[13] L. Hedin, "New method for calculating the one-particle Green's function with application to the electron-gas problem," *Phys. Rev.*, vol. 139, pp. A796–A823, Aug. 1965.

[14] F. Aryasetiawan and O. Gunnarsson, "The GW method," *Rep. Prog. Phys.*, vol. 61, p. 237, 1998.

[15] J. N. Murrell and A. J. Harget, *Semi-Empirical Self-Consistent Molecular Orbital Theory of Molecules*. New York, NY, USA: Wiley–Interscience, 1972.

[16] D. Kienle, J. I. Cerda, and A. W. Ghosh, "Extended Hueckel theory for band structure, chemistry, and transport. I. Carbon nanotubes," *J. Appl. Phys.*, vol. 100, 2006, 043614.

[17] J. C. Slater and G. F. Koster, "Simplified LCAO method for the periodic potential problem," *Phys. Rev.*, vol. 94, pp. 1498–1524, 1954.

[18] S. Datta, *Electronic Transport in Mesoscopic System*. Cambridge, U.K.: Cambridge Univ. Press, 1995.

[19] R. Lake, G. Klimeck, R. C. Bowen, and D. Jovanovic, "Single and multi-band modeling of quantum electron transport through layered semiconductors devices," *J. Appl. Phys.*, vol. 81, pp. 7845–7869, 1997.

[20] A. Svizhenko, M. P. Anantram, T. R. Govindam, and B. Biegel, "Two-dimensional quantum mechanical modeling of nanotransistors," *J. Appl. Phys.*, vol. 91, pp. 2343–2354, 2001.

[21] M. P. Lopez Sancho, J. M. Lopez Sancho, and J. Rubio, "Highly convergent schemes for the calculation of bulk and surface green function," *J. Phys. F*, vol. 15, pp. 851–858, 1984.

[22] M. Luisier, A. Schenk, W. Fichtner, and G. Klimeck, "Atomistic simulation of nanowires in the $sp^3d^5s^*$ tight-binding formalism: From boundary conditions to strain calculations," *Phys. Rev. B*, vol. 74, Jan. 2006, 205323.

[23] S. Selberherr, *Analysis and Simulation of Semiconductor Devices*. New York, NY, USA: Springer-Verlag, 1984.

[24] K. Tomizawa, *Numerical Simulation of Submicron Semiconductor Devices*. Reading, MA, USA: Artech House, 1993.

[25] K. M. Borysenko, J. T. Mullen, E. A. Barry, S. Paul, Y. G. Semenov, J. M. Zavada, M. Buongiorno Nardelli, and K. W. Kim, "First-principles analysis of electron-phonon

interactions in graphene," *Phys. Rev. B*, vol. 81, Mar. 2010, 121412.

[26] V. Perebeinos and P. Avouris, "Inelastic scattering and current saturation in graphene," *Phys. Rev. B*, vol. 81, May 2010, 195442.

[27] A. Paussa, M. Geromel, P. Palestri, M. Bresciani, D. Esseni, and L. Selmi, "Simulation of graphene nanoscale rf transistors including scattering and generation/recombination mechanisms," in *Proc. IEEE Int. Electron Devices Meeting*, Dec. 2011, pp. 11.7.1–11.7.4.

[28] M. Bresciani, P. Palestri, D. Esseni, and L. Selmi, "Simple and efficient modeling of the EK relationship and low-field mobility in graphene nano-ribbons," *Solid-State Electron.*, vol. 54, no. 9, pp. 1015–1021, 2010.

[29] A. Betti, G. Fiori, and G. Iannaccone, "Full band assessment of phonon-limited mobility in graphene nanoribbons," in *Proc. IEEE Int. Electron Devices Meeting*, Dec. 2010, pp. 32.2.1–32.2.4.

[30] A. Betti, G. Fiori, and G. Iannaccone, "Strong mobility degradation in ideal graphene nanoribbons due to phonon scattering," *Appl. Phys. Lett.*, vol. 98, no. 21, pp. 212111-1–212111-3, May 2011.

[31] A. Betti, G. Fiori, and G. Iannaccone, "Drift velocity peak and negative differential mobility in high field transport in graphene nanoribbons explained by numerical simulations," *Appl. Phys. Lett.*, vol. 99, 2011, 242108.

[32] G. Pennington and N. Goldsman, "Semiclassical transport and phonon scattering of electrons in semiconducting carbon nanotubes," *Phys. Rev. B*, vol. 68, 2003, 045426.

[33] M. G. Ancona, "Electron transport in graphene from a diffusion-drift perspective," *IEEE Trans. Electron Devices*, vol. 57, no. 3, pp. 681–689, Mar. 2010.

[34] J. K. David, L. F. Register, and S. K. Banerjee, "Semiclassical Monte Carlo analysis of graphene FETs," *IEEE Trans. Electron Devices*, vol. 59, no. 4, pp. 976–982, Apr. 2012.

[35] D. Jimenez, "Explicit drain current, charge and capacitance model of graphene field-effect transistors," *IEEE Trans. Electron Devices*, vol. 58, no. 12, pp. 4377–4383, Dec. 2011.

[36] I. Meric, M. Y. Han, A. F. Young, B. Ozyilmaz, P. Kim, and K. L. Shepard, "Current saturation in zero-bandgap, top-gated graphene field-effect transistors," *Nature Nanotechnol.*, vol. 3, no. 11, pp. 654–659, 2008.

[37] P. Zhao, M. Choudhury, K. Mohanram, and J. Guo, "Computational model of edge effects in graphene nanoribbon transistors," *Nano Res.*, vol. 1, pp. 395–402, 2008, DOI: 10.1007/s12274-008-8039-y.

[38] M. Lundstrom, "Elementary scattering theory of the Si MOSFET," *IEEE Electron Device Lett.*, vol. 18, no. 7, pp. 361–363, Jul. 1997.

[39] D. Jimenez, "A current, voltage model for Schottky-Barrier graphene-based transistors," *Nanotechnology*, vol. 19, no. 34, 2008, 345204.

[40] P. Michetti, G. Mugnaini, and G. Iannaccone, "Analytical model of nanowire FETs in a partially ballistic or dissipative transport regime," *IEEE Trans. Electron Devices*, vol. 56, no. 7, pp. 1402–1410, Jul. 2009.

[41] P. Michetti and G. Iannaccone, "Analytical model of one-dimensional carbon-based Schottky-Barrier transistors," *IEEE Trans. Electron Devices*, vol. 57, no. 7, pp. 1616–1625, Jul. 2010.

[42] G. Mugnaini and G. Iannaccone, "Physics-based compact model of nanoscale MOSFETs—Part I: Transition from drift-diffusion to ballistic transport," *IEEE Trans. Electron Devices*, vol. 52, no. 8, pp. 1795–1801, Aug. 2005.

[43] G. Mugnaini and G. Iannaccone, "Physics-based compact model of nanoscale MOSFETs—Part II: Effects of degeneracy on transport," *IEEE Trans. Electron Devices*, vol. 52, no. 8, pp. 1802–1806, Aug. 2005.

[44] H. Wang, A. Hsu, J. Kong, D. A. Antoniadis, and T. Palacios, "Compact virtual-source current voltage model for top- and back-gated graphene field-effect transistors," *IEEE Trans. Electron Devices*, vol. 58, no. 5, pp. 1523–1533, May 2011.

[45] S. Zhou, G.-H. Gweon, A. Fedorov, P. First, W. de Heer, D.-H. Lee, F. Guinea, A. Castro Neto, and A. Lanzara, "Substrate-induced bandgap opening in epitaxial graphene," *Nature Mater.*, vol. 6, no. 10, pp. 770–775, 2007, DOI: 10.1038/nmat2003.

[46] V. Ryzhii, M. Ryzhii, A. Satou, T. Otsuji, and N. Kirova, "Device model for graphene bilayer field-effect transistor," 2008. [Online]. Available: http://arXiv:0812.4490

[47] M. Cheli, G. Fiori, and G. Iannaccone, "A semianalytical model of bilayer-graphene field-effect transistor," *Electron Devices, IEEE Trans.*, vol. 56, no. 12, pp. 2979–2986, Dec. 2009.

[48] M. Cheli, P. Michetti, and G. Iannaccone, "Model and performance evaluation of field-effect transistors based on epitaxial graphene on sic," *IEEE Trans. Electron Devices*, vol. 57, no. 8, pp. 1936–1941, Aug. 2010.

[49] P. Michetti, M. Cheli, and G. Iannaccone, "Model of tunneling transistors based on graphene on SiC," *Appl. Phys. Lett.*, vol. 96, no. 13, pp. 133508–133508-3, Mar. 2010.

[50] J. Hass, W. A. de Heer, and E. H. Conrad, "The growth and morphology of epitaxial multilayer graphene," *J. Phys., Condensed Matter*, vol. 20, no. 32, 2008, 323202.

[51] Y.-W. Son, M. L. Cohen, and S. G. Louie, "Energy gaps in graphene nanoribbons," *Phys. Rev. Lett.*, vol. 97, Nov. 2006, 216803.

[52] L. Yang, M. L. Cohen, and S. G. Louie, "Excitonic effects in the optical spectra of graphene nanoribbons," *Nano Lett.*, vol. 7, no. 10, pp. 3112–3115, 2007.

[53] L. Yang, C.-H. Park, Y.-W. Son, M. L. Cohen, and S. G. Louie, "Quasiparticle energies and band gaps in graphene nanoribbons," *Phys. Rev. Lett.*, vol. 99, Nov. 2007, 186801.

[54] M. Y. Han, B. Özyilmaz, Y. Zhang, and P. Kim, "Energy band-gap engineering of graphene nanoribbons," *Phys. Rev. Lett.*, vol. 98, May 2007, 206805.

[55] S. Reich, J. Maultzsch, C. Thomsen, and P. Ordejón, "Tight-binding description of graphene," *Phys. Rev. B*, vol. 66, Jul. 2002, 035412.

[56] K. Nakada, M. Fujita, G. Dresselhaus, and M. S. Dresselhaus, "Edge state in graphene ribbons: Nanometer size effect and edge shape dependence," *Phys. Rev. B*, vol. 54, pp. 17954–17961, Dec. 1996.

[57] X. Wang, Y. Ouyang, X. Li, H. Wang, J. Guo, and H. Dai, "Room-temperature all-semiconducting sub-10-nm graphene nanoribbon field-effect transistors," *Phys. Rev. Lett.*, vol. 100, 2008, 206803.

[58] Y. Yang and R. Murali, "Impact of size effect on graphene nanoribbon transport," *IEEE Electron Device Lett.*, vol. 31, no. 3, pp. 237–239, Mar. 2010.

[59] A. Cresti, N. Nemec, B. Biel1, G. Niebler, F. Triozon, G. Cuniberti, and S. Roche, "Charge transport in disordered graphene-based low dimensional materials," *Nano Res.*, vol. 1, pp. 361–394, 2008.

[60] A. Cresti, A. Lopez-Bezanilla, P. Ordejan, and S. Roche, "Oxygen surface functionalization of graphene nanoribbons for transport gap engineering," *ACS Nano*, vol. 5, no. 11, pp. 9271–9277, 2011.

[61] B. Biel, X. Blase, F. Triozon, and S. Roche, "Anomalous doping effects on charge transport in graphene nanoribbons," *Phys. Rev. Lett.*, vol. 102, Mar. 2009, 096803.

[62] A. Betti, G. Fiori, and G. Iannaccone, "Atomistic investigation of low-field mobility in graphene nanoribbons," *IEEE Trans. Electron Devices*, vol. 58, no. 9, pp. 2824–2830, Sep. 2011.

[63] I. Deretzis, G. Fiori, G. Iannaccone, and A. La Magna, "Effects due to backscattering and pseudogap features in graphene nanoribbons with single vacancies," *Phys. Rev. B*, vol. 81, Feb. 2010, 085427.

[64] M. Evaldsson, I. V. Zozoulenko, H. Xu, and T. Heinzel, "Edge-disorder-induced anderson localization and conduction gap in graphene nanoribbons," *Phys. Rev. B*, vol. 78, Oct. 2008, 161407.

[65] T. Fang, A. Konar, H. Xing, and D. Jena, "Mobility in semiconducting graphene nanoribbons: Phonon, impurity, and edge roughness scattering," *Phys. Rev. B*, vol. 78, Nov. 2008, 205403.

[66] D. C. Elias, T. M. G. Mohiuddin, R. R. Nair, S. V. Morozov, P. Blake, M. P. Halsall, A. C. Ferrari, D. W. Boukhvalov, M. I. Katsnelson, A. K. Geim, and K. S. Novoselov, "Control of graphene's properties by reversible hydrogenation: Evidence of graphane," *Science*, vol. 323, pp. 610–613, 2009.

[67] J. O. Sofo, A. S. Chaudhari, and G. D. Barber, "Graphane: A two-dimensional hydrocarbon," *Phys. Rev. B*, vol. 75, 2007, 153401.

[68] S. Lebègue, M. Klintenberg, O. Eriksson, and M. I. Katsnelson, "Accurate electronic band gap of pure and functionalized graphane from GW calculations," *Phys. Rev. B*, vol. 79, 2009, 245117.

[69] J. N. Nakamura, N. Arimura, M. Hirayama, and A. Natori, "Structural and electronic properties of the planar c-skeleton polymers," *Appl. Phys. Lett.*, vol. 94, no. 22, 2009, 223107.

[70] N. Lu, Z. Li, and J. Yang, "Electronic structure engineering via on-plane chemical functionalization: A comparison study on two-dimensional polysilane and graphane," *J. Phys. Chem. C*, vol. 113, no. 38, pp. 16741–16746, 2009.

[71] C.-K. Yang, "A metallic graphene layer adsorbed with lithium," *Appl. Phys. Lett.*, vol. 94, no. 16, 2009, 163115.

[72] G. Fiori, S. Lebègue, A. Betti, P. Michetti, M. Klintenberg, O. Eriksson, and G. Iannaccone, "Simulation of hydrogenated graphene field-effect transistors through

a multiscale approach," *Phys. Rev. B*, vol. 82, Oct. 2010, 153404.

[73] S. Bruzzone and G. Fiori, "Ab-initio simulations of deformation potentials and electron mobility in chemically modified graphene and two-dimensional hexagonal boron-nitride," *Appl. Phys. Lett.*, vol. 99, no. 22, 2011, 222108.

[74] J. Bardeen and W. Shockley, "Deformation potentials and mobilities in non-polar crystals," *Phys. Rev.*, vol. 80, pp. 72–80, Oct. 1950.

[75] M. Q. Long, L. Tang, D. Wang, L. Wang, and Z. Shuai, "Theoretical predictions of size-dependent carrier mobility and polarity in graphene," *J. Amer. Chem. Soc.*, vol. 131, pp. 17728–17729, 2009.

[76] F. Murphy-Armando, G. Fagas, and J. C. Greer, "Deformation potentials and electron-phonon coupling in silicon nanowires," *Nano Lett.*, vol. 10, pp. 869–873, 2010.

[77] C. G. Van de Walle, "Band lineups and deformation potentials in the model-solid theory," *Phys. Rev. B*, vol. 39, pp. 1871–1883, 1988.

[78] S. Takagi, A. Toriumi, and H. Tango, "On the universality of inversion layer mobility in Si MOSFETs: Part I—effects of substrate impurity concentration," *IEEE Trans. Electrone Devices*, vol. 41, no. 12, pp. 2357–2363, Dec. 1994.

[79] M. Jaiswal, C. H. Yi, X. Lim, Q. Bao, C. T. Toh, K. Ping, and L. B. Oezyilmaz, "Controlled hydrogenation of graphene sheets and nanoribbons," *ACS Nano*, vol. 5, no. 2, pp. 888–896, 2011.

[80] E. McCann and V. I. Falko, "Landau-level degeneracy and quantum hall effect in a graphite bilayer," *Phys. Rev. Lett*, vol. 96, 2006, 086805.

[81] E. McCann, "Asymmetry gap in the electronic band structure of bilayer graphene," *Phys. Rev. B*, vol. 74, 2006, 161403.

[82] H. Min, B. Sahu, S. K. Banerjee, and A. H. MacDonald, "Ab initio theory of gate induced gaps in graphene bilayers," *Phys. Rev. B*, vol. 75, Apr. 2007, 155115.

[83] J. Nilsson, A. H. Castro Neto, F. Guinea, and N. M. R. Peres, "Electronic properties of graphene multilayers," *Phys. Rev. Lett.*, vol. 97, 2006, 266801.

[84] J. Nilsson, A. H. Castro Neto, F. Guinea, and N. M. R. Peres, "Electronic properties of bilayer and multilayer graphene," *Phys. Rev. B*, vol. 78, Jul. 2008, 045405.

[85] P. R. Wallace, "The band theory of graphite," *Phys. Rev.*, vol. 71, pp. 622–634, 1947.

[86] *Chapter 2: Process Integration, Devices, and Structures*, The International Technology Roadmap for Semiconductors, 2011. [Online]. Available: http://www.itrs.net

[87] G. Fiori and G. Iannaccone, "Simulation of graphene nanoribbon field-effect transistors," *IEEE Electron Device Lett.*, vol. 28, no. 8, pp. 760–762, Aug. 2007.

[88] Y. Yoon, G. Fiori, S. Hong, G. Iannaccone, and J. Guo, "Performance comparison of graphene nanoribbon FETs with Schottky contacts and doped reservoirs," *IEEE Trans. Electron Devices*, vol. 55, no. 9, pp. 2314–2323, Sep. 2008.

[89] Y. Yoon and J. Guo, "Effect of edge roughness in graphene nanoribbon transistors," *Appl. Phys. Lett.*, vol. 91, no. 7, 2007, 073103.

[90] Y. Ouyang, S. Sanvito, and J. Guo, "Effects of edge chemistry doping on graphene nanoribbon mobility," *Surf. Sci.*, vol. 605, no. 17-18, pp. 1643–1648, 2011.

[91] S. O. Koswatta, A. Valdes-Garcia, M. B. Steiner, Y.-M. Lin, and P. Avouris, "Ultimate RF performance potential of carbon electronics," *IEEE Trans. Microw. Theory Tech.*, vol. 59, no. 10, pp. 2739–2750, Oct. 2011.

[92] B. W. Scott and J. Leburton, "Modeling of the output and transfer characteristics of graphene field-effect transistors," *IEEE Trans. Nanotechnol.*, vol. 10, no. 5, pp. 1113–1119, Sep. 2011.

[93] S. A. Thiele, J. A. Schaefer, and F. Schwierz, "Modeling of graphene metal-oxide-semiconductor field-effect transistors with gapless large-area graphene channels," *J. Appl. Phys.*, vol. 107, no. 9, 2010, 094505.

[94] A. Paussa, M. Geromel, P. Palestri, M. Bresciani, D. Esseni, and L. Selmi, "Simulation of graphene nanoscale RF transistors including scattering and generation/recombination mechanisms," in *Proc. IEEE Int. Electron Devices Meeting*, Dec., pp. 11.7.1–11.7.4.

[95] J. Chauhan, L. Liu, Y. Lu, and J. Guo, "A computational study of high-frequency behavior of graphene field-effect transistors," *J. Appl. Phys.*, vol. 111, no. 9, 2012, 094313.

[96] I. Imperiale, S. Bonsignore, A. Gnudi, E. Gnani, S. Reggiani, and G. Baccarani, "Computational study of graphene nanoribbon FETs for RF applications," in *Proc. IEEE Int. Electron Devices Meeting*, Dec., pp. 32.3.1–32.3.4.

[97] I. Imperiale, A. Gnudi, E. Gnani, S. Reggiani, and G. Baccarani, "High-frequency analog GNR-FET design criteria," in *Proc. Eur. Solid-State Device Res. Conf.*, Sep. 2011, pp. 303–306.

[98] Y. Wu, Y. Lin, A. A. Bol, K. A. Jenkins, F. Xia, D. B. Farmer, Y. Zhu, and P. Avouris, "High-frequency, scaled graphene transistors on diamond-like carbon," *Nature*, vol. 472, no. 7341, pp. 74–78, Apr. 2011.

[99] B. N. Szafranek, G. Fiori, D. Schall, D. Neumaier, and H. Kurz, "Current saturation and voltage gain in bilayer graphene field effect transistors," *Nano Lett.*, vol. 12, no. 3, pp. 1324–1328, 2012.

[100] G. Fiori and G. Iannaccone, "Insights on radio frequency bilayer graphene FETs," in *Proc. IEEE Int. Electron Devices Meeting*, Dec., pp. 17.3.1–17.3.4.

[101] G. Fiori, A. Betti, S. Bruzzone, and G. Iannaccone, "Lateral graphene-HBCN heterostructures as a platform for fully two-dimensional transistors," *ACS Nano*, vol. 6, no. 3, pp. 2642–2648, 2012.

[102] L. Ci, L. Song, C. Jin, D. Jariwala, D. Wu, Y. Li, A. Srivastava, Z. F. Wang, K. Storr, L. Balicasa, F. Liu, and P. M. Ajayan, "Atomic layers of hybridized boron nitride and graphene domains," *Nature Mater.*, vol. 9, pp. 430–435, 2010.

[103] G. Fiori and G. Iannaccone, "On the possibility of tunable-gap bilayer graphene," *IEEE Electron Device Lett.*, vol. 30, no. 3, pp. 261–264, Mar. 2009.

[104] G. Fiori and G. Iannaccone, "Ultralow-voltage bilayer graphene tunnel FET," *IEEE Electron Device Lett.*, vol. 30, no. 10, pp. 1096–1098, Oct. 2009.

ABOUT THE AUTHORS

Gianluca Fiori received the M.S. degree in electrical engineering and the Ph.D. degree from the Università di Pisa, Pisa, Italy, in 2001 and 2005, respectively.

In autumn 2002, he visited Silvaco International, developing quantum models, which are currently implemented in the commercial simulator Atlas by Silvaco. In summers 2004, 2005, and 2008, he visited Purdue University, West Lafayette, IN, USA, where he worked on models for the simulation of transport in nanoscaled devices. Since December 2007, he has been an Assistant Professor with the Dipartimento di Ingegneria dell'Informazione, Università di Pisa. His main field of activity includes the development of models and codes for the simulations of ultrascaled semiconductor devices.

Giuseppe Iannaccone (Senior Member, IEEE) received the M.S. and Ph.D. degrees in electrical engineering from the University of Pisa, Pisa, Italy, in 1992 and 1996, respectively.

He is a Professor of Electronics at the University of Pisa. His interests include nanoelectronics and semiconductor devices, the development of device modeling and TCAD tools, and the design of extremely low-power circuits and systems for RFID and ambient intelligence scenarios. He has published more than 160 papers in peer-reviewed journals, receiving in excess of 1700 citations from ISI-WoS, and more than 110 papers in proceedings of international conferences. He has coordinated a few European and National Projects involving multiple partners and has acted as the Principal Investigator in several research projects funded by public agencies at the European and national levels and by private organizations. He is actively involved in technology transfer projects and in public outreach. Prior to joining the University of Pisa in 1996, he was a permanent researcher with the Italian National Research Council.